

Multispecies colonisation and surface erosion on A106GB industry-finished steel used in heat exchangers

Alicia Prithiraj^a, Shepherd Tichapondwa^a, Jackie Nel^b and Evans Chirwa^a

^aDepartment of Chemical Engineering, Faculty of Engineering, Built Environment and Information Technology, University of Pretoria, Pretoria, South Africa; ^bDepartment of Physics, Faculty of Natural and Agricultural Sciences, University of Pretoria, Pretoria, South Africa

ABSTRACT

Multispecies bacterial attachment to carbon steel surfaces is not fully understood; for example, as to why the attachment of certain bacteria influences corrosion. In this study, finished steel, A 106GB was exposed to a mixed bacterial culture in a batch reactor system at a constant temperature of 35°C to evaluate the corrosion rate with and without bacterial influence. Cultures collected from the cooling tower site were exposed to coupons and were grown in a batch reactor. Atomic force microscopy (AFM) was used to obtain roughness parameters. Surface morphology and colonisation patterns were observed by scanning electron microscopy (SEM). 16S *rDNA* sequencing indicated predominance of *Pseudomonas* sp. and *Clostridium* sp. on the rough surfaces. Cell colonisation of surfaces showed no time-related differences, with differences observed on surface roughness parameters. Intergranular and uniform corrosion was observed. The smooth finished steel surface performed best in resisting corrosion.

ARTICLE HISTORY

Received 15 October 2023
Accepted 28 February 2024

KEYWORDS


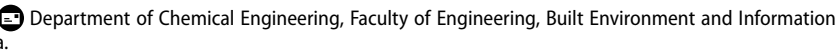
Multispecies colonisation; carbon steel; petrochemical industry; heat exchangers; atomic force microscopy


Introduction

Microbial communities in complex environments typically exist in syntropic synergy in order to optimise utilisation of resources. Microbial cultures growing on metal surfaces can facilitate corrosion reactions and erosion of surface layers [1]. Bacterial attachment is still considered one of the challenges in bioengineering applications mainly due to the complex initial cell attachment dynamics which involves deposition of exopolysaccharides (EPS) and complex interactions across the cell/biofilm matrices [2,3]. The important factors that influence initial bacterial attachment to a surface including the bacterial cell in a planktonic state are the cell appendages, pH and temperature, attachment proteins and EPS excretion [4]. Following the attachment stage, multiplication and division of the bacteria will commence and this adds to the build-up of the biofilm. EPS is the driving factor of biofilm formation in most cases [5]. Biofilm formation begins with the genetically mediated deposition of EPS which creates a protective layer for bacteria that eventually use the near surface ecosystem as a niche [6]. Bacterial attachment on

metallic surfaces have shown to affect the corrosion kinetics either by corroding or protecting the steel, it was reported that during early bacterial attachment stages high corrosion rates are observed [7,8]. Due to the accelerated corrosion and downtime experienced in the petrochemical environment, it is crucial that early colonisers are understood.

An industrial study by Prithiraj et al. [9], demonstrated that attachment of a mixed bacterial culture had an influence on the corrosion rate of industry standard steel. Zhu et al. [10] further challenged that the attachment of specific species to industry finished steel together with bacterial metabolic functioning could influence the corrosion rate. The industrial study conducted by Zhu et al. [10] posited that *Pseudomonas* sp. and *Clostridium* sp. were capable of producing organic acids thereby accelerating corrosion rate. In an environmental corrosion study conducted by Procópio [11], it was evidenced that Firmicutes (*Clostridium* sp.) were responsible for high corrosion rates on steel. However, these studies did not investigate and identify the preferential attachment of these species to a surface.

CONTACT Alicia Prithiraj  alicia.prithiraj@gmail.com 

 Supplemental data for this article can be accessed online at <https://doi.org/10.1080/13102818.2024.2326292>.

© 2024 The Author(s). Published by Informa UK Limited, trading as Taylor & Francis Group.

This is an Open Access article distributed under the terms of the Creative Commons Attribution License (<http://creativecommons.org/licenses/by/4.0/>), which permits unrestricted use, distribution, and reproduction in any medium, provided the original work is properly cited. The terms on which this article has been published allow the posting of the Accepted Manuscript in a repository by the author(s) or with their consent.

Surface modifications to reduce attachment of bacterial cells to a surface have been studied for decades across different fields. A recent study on metallic biomaterials gave insight on antipathogenic surface modifications to control infections in humans and highlighted that surface area and roughness significantly increases bacterial colonisation and biofilm formation [12,13]. Other studies showed the efficacy of marine bacteria *Cobetia marina* and seaweed spores *Ulva linza* in facilitating colonisation and potential impacts on corrosion of metallic surfaces [14]. Some studies also evaluated attachment of a few strains of bacteria to a rough or smooth surface, and results were rather inconsistent [8,15].

There is limited research that has been conducted on the preferential attachment of a mixed bacterial culture to industrial standard steels, which contributes to corrosion in the petrochemical environment. Two specific works in dentistry studied multispecies colonisation on rough and smooth finished dental material [16,17]. These studies used different methods to evaluate surface roughness and the results were rather contrasting from each other.

Electron microscopy and confocal laser scanning microscopy have been traditionally used to count bacterial cells at the surface [17]. However, all of these methods are imprecise, indirect and tedious [18]. There are reports of single-strain bacteria exposed to a given surface for a short period of time which allows for visibility of the bacteria under the microscope [19]. However, these conditions do not reflect a multispecies system. 16S *rDNA* sequencing with qPCR was used in a study by Park et al. [17] to quantify bacterial cell attachment to a surface. Third-generation sequencing can also give more insight into microbial species colonising steel.

The latest development in atomic force microscopy (AFM) offers new opportunities in characterising surfaces [18] by examining bacterial attachment and surface roughness at atomic, nanoscale and microscale levels. Although time consuming, AFM is able to quantitatively evaluate a given surface.

It is important to understand how multiple bacterial species interact and attach to the steel specifications to recommend an optimum surface finish and cut costs. This study used third generation sequencing together with absolute qPCR and AFM to provide new insights into bacterial colonisation of industry finished carbon steel tube material. This study establishes formative standards when implementing new tube bundles in heat exchangers used for cooling water service, and broaden the comparison to literature, while presenting a better understanding of multispecies colonisation to surfaces. The study also highlighted key role

players responsible for corrosion in the petrochemical industry.

Materials and methods

Experimental set-up

A stainless-steel perforated mesh designed to collect bacteria, with dimensions 0.178 mm x 12.7 mm x 76.2 mm was inserted *in situ* as a coupon rack in a cooling tower circulation pipeline at the petrochemical plant in South Africa (Supplemental Figures S1 and S2). The mesh was left in place for a period of 11 months. Cooling water was directly transported from the cooling tower to the coupon rack at low flow. The coupon rack was designed to hold only one biofilm mesh. The mesh was removed from the coupon rack using sterilised tweezers and inserted in a sterile sample bag containing the cooling tower water. The bag with the mesh was transported to an on-site microbiology laboratory. Upon arrival at the laboratory, the mesh was immediately transferred into a batch reactor containing autoclaved prepared media with sterilised carbon steel alloys.

Bacterial cultivation

The batch reactor was placed in an incubator equipped with a thermostat and set at a constant temperature of 35°C to simulate the cooling tower temperature conditions. The bacteria on the coupon surfaces were grown anaerobically and the batch reactor was only opened to remove the alloys, however, cooling towers operate as open systems. Modified batch mineral medium was prepared from 0.501 g KH_2PO_4 , 1.000 g NH_4Cl , 4.502 g Na_2SO_4 , 0.005 g $\text{CaCl}_2 \cdot 2\text{H}_2\text{O}$, 0.062 g $\text{MgSO}_4 \cdot 7\text{H}_2\text{O}$, 12.012 g 50% solution sodium lactate, 1.001 g yeast extract, 0.004 g $\text{FeSO}_4 \cdot 7\text{H}_2\text{O}$, 5.002 g $\text{Na}_3\text{C}_6\text{H}_5\text{O}_7$ sodium citrate mixed in 1.00 L distilled water to simulate the mineral rich water quality of river water fed to the cooling towers with minimal carbon sources. The initial pH of 6.52 was adjusted to 7 using 5 M NaOH. The adjustment of pH was conducted for consistence with other studies on the impact of metal finish on bacterial attachment [10]. Day 3, 6 and 13 were chosen for this study based on the growth phases (lag, exponential and death) from previous bacterial growth rate studies [20].

Alloy preparation

Carbon steel coupons, measuring 1 cm by 1 cm, were polished to two different finishes. The rough and smooth

surfaces were polished to 400 grit finish using silicon carbide waterproof paper and 3-micron polish, respectively. The coupons were polished using an Automatic Polishing Machine (Struers Tegramin-30, United States, Cleveland, Ohio) for 3 min, using a force of 35 N at 300 revolutions per minute. Carbon steel alloys were fastened on cable ties, rinsed with acetone and sterilised for 1 h using 70% ethanol. All work was conducted under a laminar flow hood. The fastened coupons were inserted into the batch reactor containing the media inoculated with a mixed bacterial culture. Coupons were rinsed three times to remove loosely attached bacteria before evaluation under the microscopes.

Surface study

The morphological properties of the uncoated samples (in a hydrated state) as well as the elemental composition and distribution mapping of the surface in abiotic (without bacteria) and biotic (with bacteria) conditions were studied using a Crossbeam 540 scanning electron microscope (Oxford Instruments, Zeiss Gemini 2), with an accelerating voltage of 5 kV coupled with an energy dispersive X-ray (EDX). The hydrated bacterial coupons were dried by placing on a paper towel (to absorb any excess media dripping from the coupon) on the side that was not scanned and were transferred to a platform (stage) for scanning. AFM was conducted on smooth and rough surfaces before and after exposure on the multispecies biofilm over 3, 6 and 13 days on alloy A to obtain roughness parameters. Five fields of vision were evaluated on each coupon and standard deviations were obtained based on the mean. Some coupons were easier to scan than others (dependent on surface roughness). The samples were studied in a Bruker Dimension Icon AFM with ScanAsyst (Germany). A micro-Raman Confocal Microscope (WITec Alpha 300 RAS+, Germany) was used to characterise corrosion products on the surface with the multispecies biofilm layer. The Raman was configured at a 532 nm laser at a laser power of 0.102 mW and an integration time of 15 min. The FTIR spectrum was measured using Fourier Transform Infrared spectroscopy (FTIR) (Spectrum 65, Perkin Elmer, Waltham, Massachusetts, United States) in the range of 4000–1500 cm^{-1} . The sample was placed directly under the probe to obtain the spectra, without coating the sample. The wavenumber was determined for areas where peaks were observed. Raman spectroscopy analysis has been established as a reliable instrument for corrosion studies either in single layer or multi-layer surface characteristics evaluation [21].

Similarly, FTIR in transmission mode is able to give more information about the exposed steel due to the penetration of the infrared radiation from the probe and a non-destructive technique.

Separate alloys (six alloys) for 16S *rDNA* analysis were removed under the laminar flow hood. Alloys were gently rinsed 3 times with sterilised distilled water to remove loosely attached bacteria and swabbed on the polished side (middle of the coupon) using a sterile swab. The sterile swab tube was sealed with parafilm and stored in a freezer for 13 days before analysis was conducted. This was done to identify the early (day 3), middle (day 6) and late colonisers (day 13) on each surface.

Species identification

Genomic DNA (*gDNA*) extraction of the bacterial swabs was done by using ZymoBIOMICS DNA Mini-preparation kit, D4300 Zymo (Zymo Research). The extracted *gDNA* was amplified in a PCR (Polymerase chain reaction) machine (Eppendorf Mastercycler Nexus Gradient), using a universal primer pair 27F and 1492R as previously described [22]. This was done in order to target the V1 and V9 region of the bacterial 16S *rDNA* gene. The resulting amplicons were barcoded with PacBio M13 barcodes for multiplexing through limited PCR. The resulting barcoded amplicons were quantified and a pooled equimolar and AMPure PB bead-based purification step was then performed. The PacBio SMRTbell library was prepared from the pooled amplicons following the manufacturer's protocol. Sequencing primer annealing and polymerase binding was done following the SMRTlink software protocol to prepare the library for sequencing on the PacBio Sequel IIe system [23].

Samples were sequenced on the Sequel system *via* PacBio software. Raw subreads were processed through the SMRTlink (v9.0) software and *usearch*. The taxonomic information was determined based on the Ribosomal database project 16s database v16. The taxa classification percentage abundance reports were created using an inhouse python script. Highly accurate reads were processed *via* Circular Consensus Sequences (CCS) and *Vsearch* software to produce a metagenomic report with species read count and percentage abundance.

Another set of six alloys from the same media were gently rinsed and swabbed under sterile conditions and used to obtain bacterial levels on the surface. The quantitative polymerase chain reaction (qPCR) was used. The standard curve (Supplemental Figures S3 and S4) was generated using a serial dilution of the pGEM-T plasmid from 0.1 ng to 0.1 fg.

The qPCR was then performed in 96 well plates with Luna Universal qPCR Master Mix (New England Biolabs, Ipswich, MA, USA) using dye-based qPCR assay. Each reaction contained 1 µl of DNA template, 0.25 µm forward (TCCTACGGGAGGCAGCAGT) and reverse (GGACTACCAGGGTATCTAATCCTGTT) primers and 1 X Luna Universal qPCR Master mix (NEB M3003). The reactions were run on a CFX96 Real-Time PCR System (Bio-Rad) following a three-step PCR program. The cycling conditions were 1 X (95 °C for 5 min), 40 X (95 °C for 10 s; 60 °C for 15 s and 72 °C for 20 s) followed by a melt curve analysis (Supplemental Figure S5) from 60 °C to 95 °C in 0.2 °C increments. Three technical replicates were run for each DNA sample (Supplemental Table S1). Amplification of different input templates were evaluated based on the quantification cycle (Cq) value. The absolute copy number was calculated using the formulas in the supplementary file. The average Cq values were plotted against the absolute copy number of standards and standard curves which were generated by a linear regression of the plotted points (Supplemental Figures S3 and S4). The absolute copy number for the bacterial strains was calculated based on the standard curve.

Corrosion rate

Duplicate batch systems were used to evaluate corrosion of carbon steel grade A: A 106GB. One of the systems was inoculated with bacteria and the other one was without bacteria. Equation 1 was used to determine corrosion rate (mm/y) using NACE standards 169-2000 Item no.21200, ASTM G1-72 [24] and ASTM D2688-70 [25]. These laboratory methods and standards are used for preparing, cleaning, and evaluating corrosion test specimens, and testing for corrosivity of water in the absence of heat transfer (weight loss methods).

$$Cr = \frac{(W_1 - W_4) \times 365 \times 100}{\rho_c \cdot A \cdot t} \quad (1)$$

where Cr is corrosion rate (mm/y), W_1 is the initial weight of coupon (g), W_4 is the final weight of coupon (g), ρ_c is the coupon density (g/dm³), A is the surface area (dm²) and t is time in days. Six carbon steel alloys were initially weighed and placed in the batch reactors. The cleaning and weighing process after media exposure was conducted by placing the alloys in 32% HCl solution for 25 min with 0.34 mL Armohib corrosion inhibitor as well as 10% caustic solution to obtain the final weight. Coupons were further soaked in acetone and brushed lightly with a soft brush under

flowing water after every treatment and dried at 105 °C before weighing. The soft brush was used to remove any visible biofilm or corrosion product on the surface.

Etching of the alloy

Microstructural analysis of a separate alloy A 106GB was conducted conforming to standards ASTM 407 and ASTM E3 [9]. The specimen was mounted with a multifast Phenolic hot mount resin using a Struers mounting press (CitoPress – 15, Ballerup, Denmark) set at 180 °C. The mounted carbon steel alloy was polished with a polish disc from 220 grit to 1200 grit and cleaned with acetone. To reveal the microstructure, the alloy was etched by immersing in nital (2 mL HNO₃ and 98 mL ethyl alcohol) for 15 s, then cleaned with water and acetone and observed under an optical microscope (Nikon Eclipse MA 200, Tokyo, Japan).

Statistical analysis

Mean values and corresponding 95% confidence intervals were calculated to determine the difference between rough and smooth surfaces at respective bacterial colonisation times. Time-related differences in roughness values were determined with a paired t-test. One-way analysis of variance (ANOVA) was performed on the surface finishes and corrosion rates to establish differences between the differently finished alloys. Significance was set at 95%. The bacterial species abundance was evaluated using Permutational analysis of variance (PERMANOVA) in PRIMER 7. The analysis was conducted to determine the differences in bacterial species abundance between sample surfaces. Percentage data was transformed using the square-root. The resemblance and PERMANOVA design was conducted using the Bray-Curtis similarity, unrestricted permutation method. The linear relationship between species abundance and corrosion rate was evaluated using Pearson's correlation and regression to obtain significance. Significance was set at 95%. One-way ANOVA was performed on the absolute copy number to obtain the difference in bacterial levels between the rough and smooth surfaces.

Results

Bacterial colonisation

The first step was to analyse the bacterial colonisation on the surfaces. Bacteria could be visualised by SEM on day 3. Table 1 presents the surface assessment of the bacterial species abundance using rDNA gene

sequencing. The early, middle and late colonizers are presented for rough and smooth surfaces. In this study there were no significant time-related differences in the colonisation for both surface finishes p (perm) >0.05 . Further to this, the absolute qPCR results showed no significant time-related differences ($p>0.05$) in bacterial levels for both surface finishes.

During the early stages of attachment (Table 1), the abundance of *Clostridium* sp. was higher on the rough finished surfaces with a species abundance of 80.25%, than on the smooth surfaces with a species abundance of 77.76%. *Clostridium* sp. attachment may be higher on the rough finished surface due to friction at

the surface and larger surface area. Scratches and grooves observed on the rough surface range from about 1–1.5 μm (Figure 1b), whereas the bacteria generally have a width of about 0.5 μm . This then would enhance the attachment of cells to the surface [13,17]. The topographical dynamics of the rough and smooth surfaces are produced by the grit size of the silicon carbide paper and polish, making the surfaces distinctly different; the smooth surface indicated scratches of about 0.5 μm (Figure 1a) or less. Several species of the *Clostridium* genus contributed to biofilm development and possessed metal-related metabolic activities, initiating attachment to the steel surface at early

Table 1. Bacterial abundance on the alloy surface determined by *rDNA* gene sequencing, with top 5 species.

Smooth surface*	Species read count	% [†]	Smooth surface*	Species read count	% [†]	Smooth surface*	Species read count	% [†]
Total early colonisers (day 3)	1425	100	Total middle colonisers (day 6)	9315	100	Total late colonisers (day 13)	9522	100
<i>Clostridium intestinale</i>	804	56.42	<i>Unknown</i>	3979	42.72	<i>Desulfotomaculum aeronauticum</i>	4548	47.76
<i>Clostridium butyricum</i>	155	10.88	<i>Clostridium butyricum</i>	2427	26.05	<i>Pseudomonas</i>	3293	34.58
<i>Clostridium metallolevans</i>	149	10.46	<i>Clostridium metallolevans</i>	1219	13.09	<i>Unknown</i>	473	4.97
<i>Unknown</i>	123	8.63	<i>Clostridium intestinale</i>	489	5.25	<i>Clostridium butyricum</i>	338	3.55
<i>Streptococcus</i>	50	3.51	<i>Methylobacterium adhaesivum</i>	187	2.01	<i>Sedimentibacter</i>	233	2.45
<i>Other species**</i>	144	10.1	<i>Other species**</i>	1014	10.88	<i>Other species**</i>	637	6.69
Rough surface*	Species read count	% [†]	Rough surface*	Species read count	% [†]	Rough surface*	Species read count	% [†]
Total early colonisers (day 3)	2486	100	Total middle colonisers (day 6)	9002	100	Total late colonisers (day 13)	9767	100
<i>Clostridium metallolevans</i>	986	39.66	<i>Pseudomonas</i>	2816	31.28	<i>Comamonas</i>	8913	91.26
<i>Clostridium intestinale</i>	702	28.24	<i>Unknown</i>	1975	21.94	<i>Desulfotomaculum aeronauticum</i>	161	1.65
<i>Clostridium butyricum</i>	307	12.35	<i>Clostridium butyricum</i>	1830	20.33	<i>Unknown</i>	159	1.63
<i>Unknown</i>	229	9.21	<i>Clostridium metallolevans</i>	854	9.49	<i>Delftia</i>	98	1.00
<i>Pseudomonas</i>	71	2.86	<i>Clostridium intestinale</i>	422	4.69	<i>Pseudomonas</i>	55	0.56
<i>Other species**</i>	191	7.68	<i>Other species**</i>	1105	12.27	<i>Other species**</i>	381	3.90

*The P-value among both groups were determined to be p (perm) >0.05 . [†] Species percentage abundance. **Other individual bacterial species amounting to less than 1 % and attached to the alloy surface.

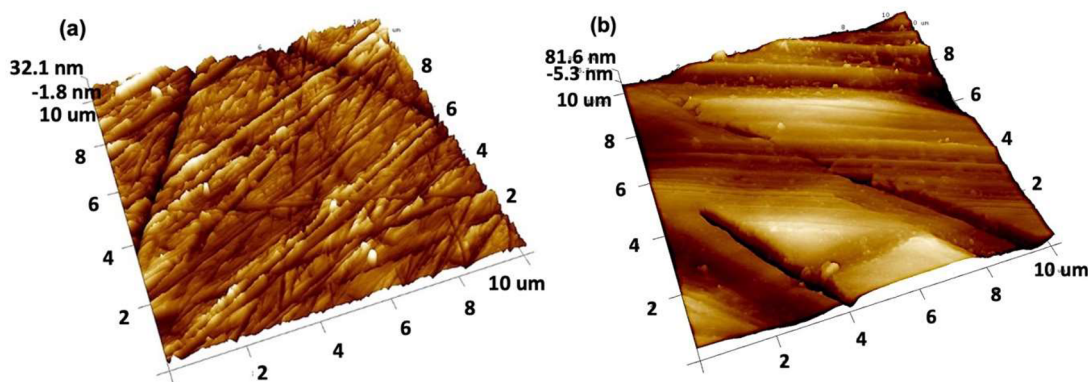


Figure 1. Three-dimensional representation of the Atomic Force micrographs of mechanically polished 3 micron (a) and 400 grit (b) finished surfaces.

attachment stages [26]. A global distribution of the 16S rRNA sequence determined for *Clostridium intestinale* (Table 1) was found in animal, aquatic, soil and plant samples (Sequence accession number: X76740). *Streptococcus* representatives were observed on day 3. Frequently seen bacteria on the surfaces were *Clostridium* sp., however, *Pseudomonas* sp. were observed on day 3 and day 6 and favoured the rough finished surface (400 grit). *Pseudomonas* sp. were observed only in the later attachment stages on the smooth surface). The presence of bacterial species *Desulfotomaculum aeronauticum* and *Delftia* at the late stages, infers that their presence may not directly impact steel corrosion at early stages. *Comamonas* sp. were evident only on day 13 rough surface and almost fully colonised the surface (91.26%). The abundant *Clostridium* sp. was reported to produce organic acids associated with corroding metals (Procopio 2021; 27]. A large number of unknown species (42.72%) were observed on the smooth surface during middle colonisation.

The results failed to reject the null hypothesis where $p(\text{perm}) > 0.05$, therefore there were no significant time-related differences in colonisation and bacterial levels ($p > 0.05$) on rough and smooth finishes. During initial colonisation (day 3), surface roughness had an influence on bacterial colonisation. The abundant *Clostridium* sp. representatives were more prevalent on the rough finished surface (Table 1). This suggested that during initial colonisation, bacteria attached to the substrate. Middle and late colonising bacteria may attach to the already present biofilm and bacteria. Surface finish no longer becomes the influencing factor, due to growth and maturation of the biofilm which is formed rapidly [17]. The results highlighted the importance of conducting third generation sequencing, and identifying the key role players at early stages which preferentially attached to the steel surface. Plots on the dependence of bacterial attachment extent as a function of surface roughness is presented in Supplemental Figures S6 and S7. In light of the findings, this study can be seen in the general

context as similar findings were observed in a multi-species study in the field of Medical Dentistry [16 and 17].

Quantitative assessment of the surface

Table 2 presents the root mean square (RMS) roughness values of alloy A before and after bacterial exposure in the batch reactor media. One-way ANOVA was conducted over 3, 6 and 13 days to determine time-related differences among the groups. On the smooth surface, the RMS roughness increased from a value of 8.68 ± 1.24 nm (before bacterial exposure) to 114.67 ± 10.69 nm (after bacterial exposure) because of initial bacterial attachment and biofilm development. However, on the rough surface during initial colonisation, the RMS roughness value was lower than the smooth surface with a value of 70.70 ± 2.1 nm. This gives indication that bacteria had likely started forming biofilm rapidly on the rough surface compared to the smooth surface, thereby producing a smoother surface initially. The presence of bacteria on a surface can give a more irregular surface finish, as the spaces between them would not be filled. This was visualised using SEM on day 3 (see below). This gives more insight into the stages of multispecies biofilm formation on a particular surface and future work on biofilm structures may be considered. The ANOVA test gave a p value of $p < 0.05$, which rejected the null hypothesis, indicating that there was a significant time-related difference in roughness parameters on the smooth and rough finished surfaces. A Student's t -test further confirmed that there were significant differences among rough and smooth groups. This concludes that multi-species colonisation with a p value of $p(\text{perm}) > 0.05$ is not proportional to surface roughness with a p value of $p < 0.05$. Similar observations were reported in a multispecies study by Park et al. [17].

Morphology of the rough and smooth surface

Figure 1a and b depict the AFM three-dimensional images of the smooth and rough finished alloys before bacterial exposure. SEM images before bacterial exposure are depicted in Figure 2a and b. Figure 3 presents the SEM images of the alloy after exposure to bacterial media. On day 3, the smooth finished alloy showed a significant increase in roughness, which was observed by qualitative assessment (Figure 3a). The attached bacterial cells were randomly orientated on the surface and not parallel to the polishing scratches. For the rough surface on day 3, the RMS roughness was

Table 2. Mean surface roughness parameters before and after bacterial exposure.

Smooth finish*	After exposure Root mean square Rq (nm)	Rough finish*	After exposure Root mean square Rq (nm)
Day 0	8.68 ± 1.24	Day 0	39.16 ± 15.87
Day 3	114.67 ± 10.69	Day 3	70.70 ± 2.1
Day 6	55.81 ± 11.70	Day 6	260.83 ± 31.35
Day 13	31.25 ± 4.61	Day 13	490.33 ± 121.32

*The p -values among both groups were determined to be < 0.05 and Student's t -test showed significant differences. ($N = 3/\text{group}$). Scan size of $10 \mu\text{m}$.

found to have increased from the unexposed value of $\sim 39.16 \pm 15.87$ nm to 70.70 ± 2.1 nm. Visually, the SEM images showed a smoother surface where few bacteria could be observed. On day 6 and 13, the rough surfaces exhibited a further increase in RMS roughness values (Table 2), which may be attributed to the complex biofilm structures including motile bacteria

dispersed on the surface of the biofilm. This was evidenced by SEM images in Figure 3f. The lower RMS roughness values seen on these days on the smooth surfaces (Figure 3c and e) did not show presence of motile bacteria, inferring a smoother surface.

The microstructure of the unexposed alloy A (Figure 4) was compared to the SEM images in Figure 5, where

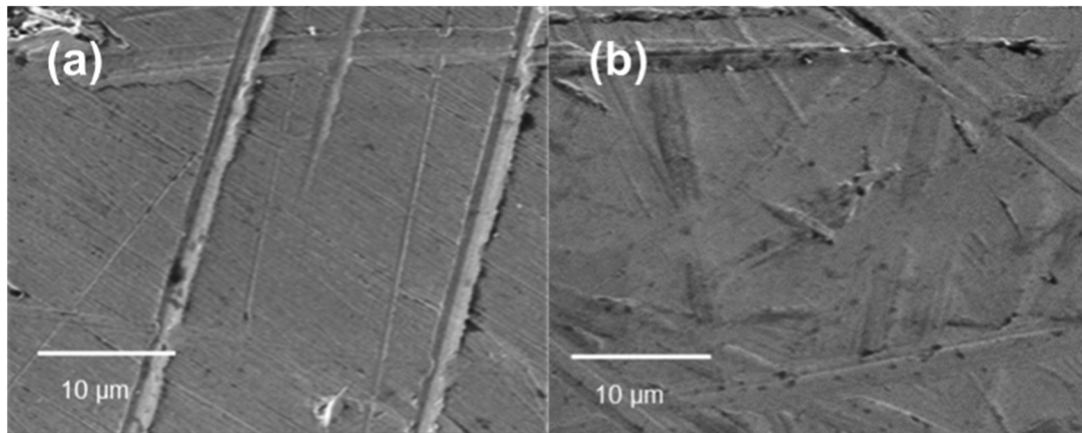


Figure 2. Representative SEM images of smooth (a) and rough (b) alloy surfaces.

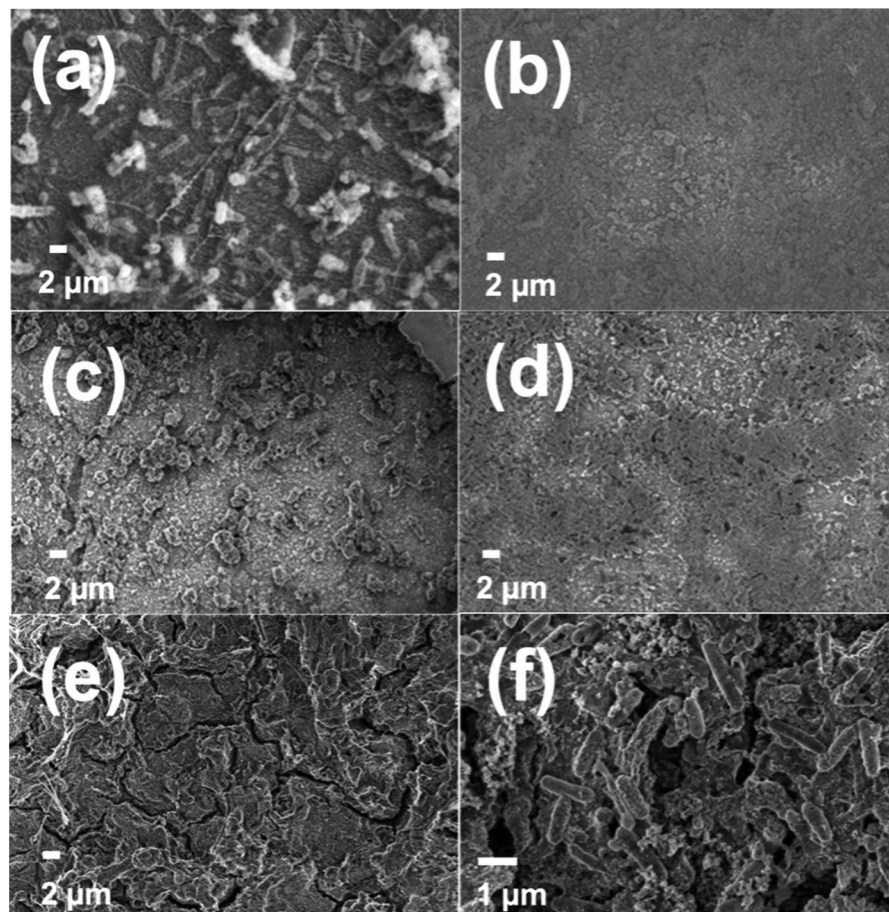


Figure 3. Scanning electron micrographs depicting the smooth surface on day 3 (a), day 6 (c) and day 13 (e) and rough surfaces on day 3 (b), day 6 (d) and day 13 (f).

the bacterial biofilm and corrosion products were cleaned from the rough and smooth surfaces and revealed intergranular and uniform corrosion. Figure 6 depicts the abiotic samples after the surface was cleaned. Figure 5a, c and e depicts the smooth surface revealing intergranular corrosion. This can be visually observed along the grain boundaries [9]. This was seen on day 3 with some damage to the grains. When compared to the abiotic system intergranular corrosion was not observed on day 3, the lamellae were clearly visible in the perlite (Figure 6a). On day 6, the grains and grain boundaries were visible in some areas of the samples exposed to bacteria, and intergranular attack could be observed (Figure 5c). In the abiotic system, there was no damage observed on the surface and the lamellae were still visible on day 6 and day 13. In the biotic system on day 13, the grain boundaries were more visible in comparison to day 6, with certain areas of localised attack to the grain. On the rough finished surfaces (Figure 5b, d and f), uniform corrosion was observed from day 3 and intergranular corrosion was observed with attack to the grain in a localised area (Figure 5b and f). This coincided with the colonisation data on day 3 (Table 1) and SEM images (Figure 3a and b). On the rough finished surfaces on day 3, 6 and 13, the type of corrosion was more uniform over the entire surface (Figure 6b, d and e). On day 13, the lamellae in the perlite could still be observed with some damage. Elemental analysis may shed some light on the compositional changes in the steel, as discussed below.

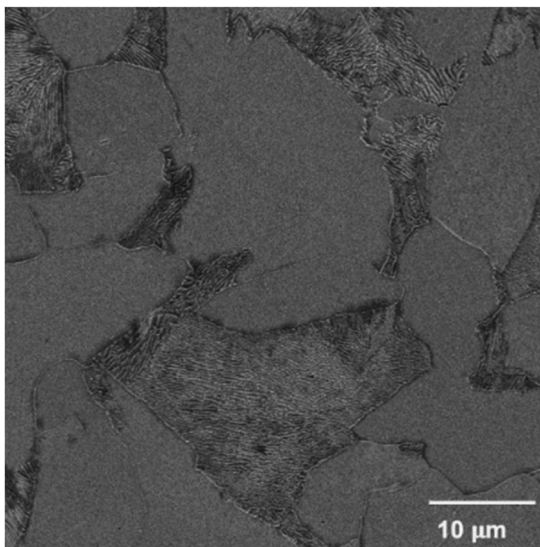


Figure 4. Scanning electron micrograph of the original etched alloy A (without batch media exposure) revealing the perlite (dark area) and ferrite (light area) phases. The lamellae can be seen in the perlite.

Elemental mapping

An elemental analysis was conducted on the alloy without exposure to batch media, conforming to ASTM E415 standards (Table 3). This was also done to confirm the grade of steel used in this study. A general observation was made on the carbon content. Before bacterial exposure, the carbon values for alloy A, in weight percent, were determined to be 0.19%, with iron being 98.29%. An elemental analysis using EDX on the SEM was then conducted after bacterial exposure. Considering the sensitivity of the instrument, this method was only used to indicate the presence of the elements. The carbon values for alloy A were observed to be 7.23% on day 3, 12.18% on day 6 and 8.52% on day 13 (Table 3). After removing the biofilm from the surface, EDX detected carbon at about 10% on day 6 (Table 4). In the abiotic system, carbon was 7.10% on day 6. The presence of the high carbon element detected by EDX analysis is commonly detected in biofilms as a principal component of bacterial cells. Moreover, metals are able to adsorb organic molecules such as yeast extract. The original iron content in Table 3 (before exposure 98.29%) was compared to the iron content after bacterial exposure (Table 4). Iron had depleted to a value as low as 46.91% on day 13. When compared to the abiotic system, iron was observed to be 90.06%. Balamurugan et al. [28] reported a similar minimum value in the firewater system containing iron-reducing bacteria (IRB) known as *Pseudomonas* sp. Among the other elements in the multispecies biofilm, sulphur was seen at the highest value of 1.9%, phosphorus at 0.33% on day 3, then further depleted to 0.11% on day 13.

The change in material composition in some instances may be attributed to the decreased sensitivity on the material due to the presence of the multispecies biofilm. Elements such as phosphorus, sulphur and chloride together with organic acids produced by bacteria are known as corrosion initiators.

Corrosion rate

The corrosion rates (Table 5) were high when the alloys were exposed to bacteria. The smooth surfaces of alloy A were seen to perform best in this system when exposed to the bacteria. There were overall reduced corrosion rates on day 13. Although *Clostridium* sp. were prevalent on all surfaces, *Pseudomonas* sp. were identified on the rough surfaces on day 3 and day 6. No significant differences in corrosion rates were observed ($p > 0.05$) in both rough and smooth groups. However, when conducting ANOVA only on day 6 rough and

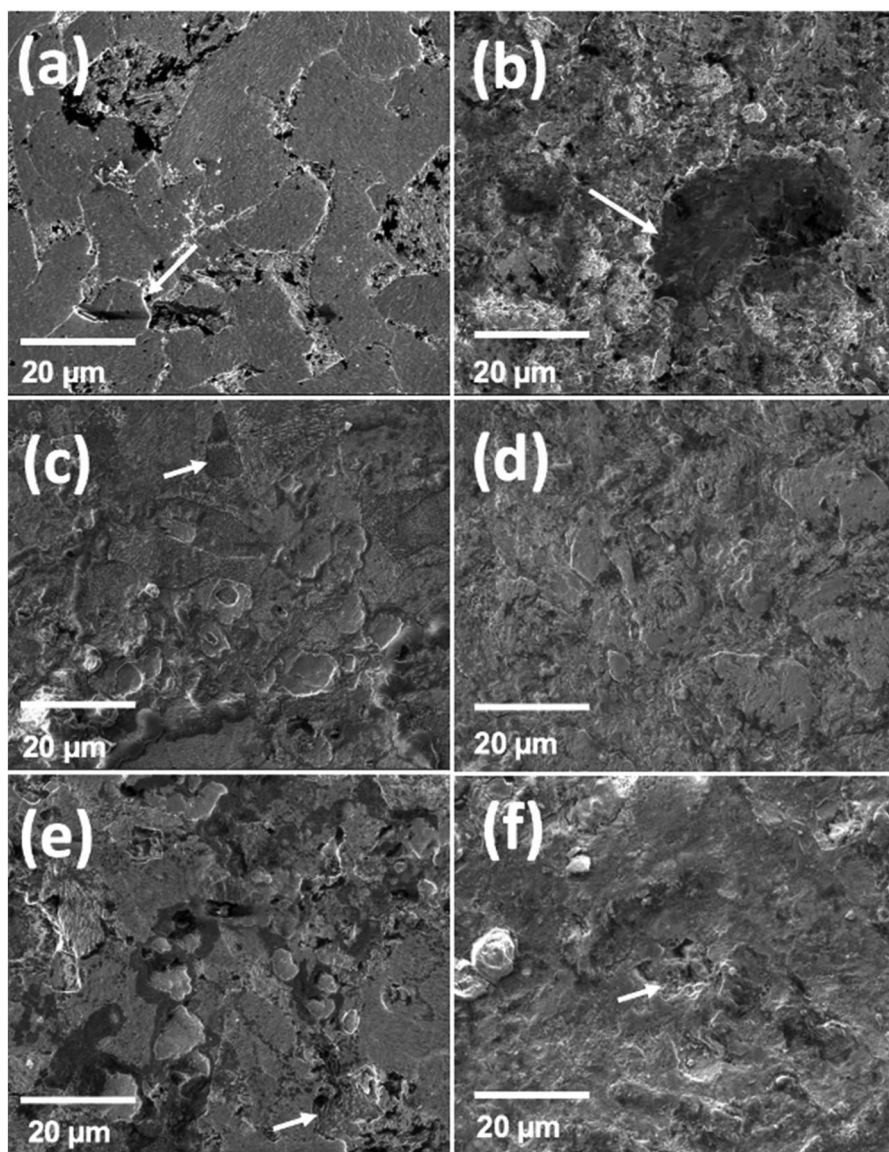


Figure 5. Scanning electron micrographs after cleaning the bacterial biofilm and corrosion products on the surfaces, depicting the smooth surface on day 3 (a), day 6 (c) and day 13 (e) and rough surfaces on day 3 (b), day 6 (d) and day 13 (f). Intergranular corrosion is indicated by the white arrows.

smooth surfaces, there was a significant difference observed ($p < 0.05$). It was observed that the increase in biofilm RMS roughness did not necessarily result in high corrosion rates of steel at different periods of exposure. This was evidenced by the RMS roughness values in [Table 2](#), where a high RMS roughness value of 490.33 ± 121.32 nm on the rough surface on day 13, showed lower corrosion rates as seen in [Table 5](#). The RMS roughness value (260.83 ± 31.35 nm) on day 6 gave a higher corrosion rate on the rough surface when compared to day 13. For the smooth surface on day 3 the RMS value was 114.67 ± 10.69 nm with a corrosion rate of 2.25 mm/y however, on day 13 the RMS roughness observed (31.25 ± 4.61 nm) gave a lower corrosion

rate (0.24 mm/y). More understanding into the spatial distribution and multispecies biofilm development on surface finishes as seen in [Supplemental Figure S8](#), and its impact on the corrosion rate is required. The correlation and regression analysis of the species abundance and corrosion rate proved that there was no significant ($p > 0.05$) linear relationship between smooth and rough surfaces.

There was an increase in the corrosion rates of the alloys when exposed to the bacterial media on days 3, 6 and 13 ([Table 5](#)), when compared the abiotic system. However, some grades of steel exhibited unusual corrosion behaviour on certain days. This challenges the hypothesis that an increase in corrosion rate would be

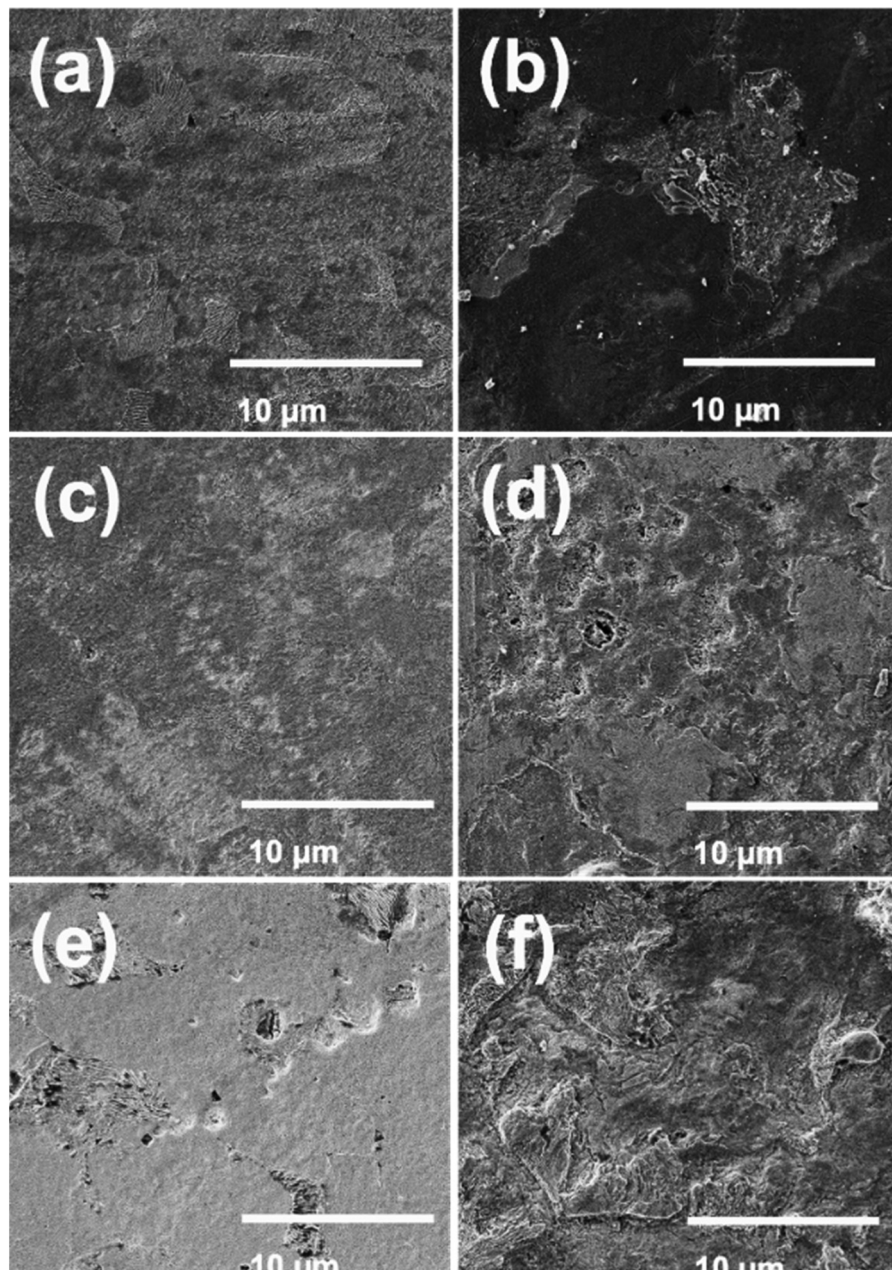


Figure 6. Scanning electron micrographs after cleaning the corrosion products on the abiotic surfaces, depicting the smooth surface on day 3 (a), day 6 (c) and day 13 (e) and rough surfaces on day 3 (b), day 6 (d) and day 13 (f).

expected in a bacterial system. In the abiotic system, the rough alloy on day 3 exhibited higher corrosion rates when compared to the abiotic smooth alloy on day 3. This occurrence was reported in a study by Kim et al. [29], where it was evidenced that increased surface roughness without microbial influence may also have an effect on the corrosion of steel. However, not as substantial as in a system with bacteria. On the contrary, in the presence of bacteria, the smooth surface on day 3 indicated higher corrosion rates when compared to the rough finished surface on day 3. This indicated corrosion resistance and was observed to be the

attachment and formation of biofilm by *Pseudomonas* sp. on day 3 (Table 1). Whereas, *Pseudomonas* sp. was not identified on the smooth surface. Biofilm formation on the rough finished surface was supported by the SEM images on day 3 (Figure 3b). There was an instance of mass increase rather than the expected mass decrease observed on smooth alloy A on day 6 (-96.5mm/y). This behaviour was not observed in the abiotic system and showed stable corrosion rates of 0.32mm/y . The mass increase observed may be due to carbon-metal bonding by acetogenic and hydrogen-producing species (*Clostridium* sp.) forming covalent bonds with iron.

Table 3. Elemental composition of smooth alloy A (without batch media exposure) and after bacterial exposure in the biotic system (with biofilm) on days 3, 6 and 13.

Elements	Alloy A before exposure*	Alloy A after exposure on day 3*(with biofilm)	Alloy A after exposure on day 6*(with biofilm)	Alloy A after exposure*on day 13*(with biofilm)
C	0.19	7.23	12.18	8.52
Fe	98.29	74.60	57.15	58.51
Si	0.26	0.22	0.21	0.17
Mn	0.87	0.00	0.00	0.93
P	0.00	0.33	0.56	0.11
S	0.00	0.24	0.33	1.89
Cr	0.10	0.00	0.00	0.00
Mo	0.10	0.00	0.00	0.00
Ni	0.02	0.24	0.27	0.27
Al	0.03	0.00	0.00	0.00
Cu	0.01	0.00	0.00	0.00
Nb	0.02	0.00	0.00	0.00
Ti	0.01	0.00	0.00	0.00
V	0.03	0.00	0.00	0.00
Cl	0.00	0.02	0.01	0.00
K	0.00	0.03	0.11	0.00
W	0.05	0.00	0.00	0.00
Na	0.02	0.47	0.78	0.00
O	0.00	16.60	28.27	29.60
Ca	0.00	0.03	0.14	0.00
Total	100	100	100	100

*Units indicated in Weight %.

Table 4. Elemental composition of the smooth alloy a of the cleaned abiotic surface (control) and cleaned biotic surface (without biofilm).

Elements	Alloy A abiotic system on day 3* (cleaned)	Alloy A abiotic system on day 6* (cleaned)	Alloy A abiotic system on day 13* (cleaned)	Alloy A after exposure on day 3* (without biofilm)	Alloy A after exposure on day 6* (without biofilm)	Alloy A after exposure on day 13* (without biofilm)
C	7.19	7.10	5.95	8.08	9.94	9.05
Fe	84.66	86.71	90.06	84.65	60.2	46.91
Mn	0.83	0.85	0.97	0.82	0.67	0.61
O	7.32	5.35	3.02	6.45	29.1	43.4
Total	100	100	100	100	100	100

*Units indicated in Weight %.

Table 5. Corrosion rates for alloy A.

Smooth Alloy A	Without bacterial exposure (smooth)*	With bacterial exposure (smooth)*	Without bacterial exposure (rough)*	With bacterial exposure (rough)*
Day 3	0.31±0.04	2.25±0.13	1.02±0.054	1.7±0.02
Day 6	0.32±0.15	-96.5±0.17	0.40±0.02	38.7±0.15
Day 13	0.29±0.03	0.36±0.13	0.24±0.02	1.20±0.05

*Units indicated in mm/y. $p > 0.05$.

Enzymes may direct the hydrogen and carbon dioxide produced by the bacteria into the acetogen metabolism where the enzyme active sites share carbon-metal bonds. Carbon-metal bonding in steel was reported by Martin [30]. It is also to be noted that in addition to the carbon-metal bonding phenomenon, surface sensitive

IR such as FTIR may be used to detect C-Fe bonds to further prove the presence of these bonds.

For rough alloy A exposed to bacteria on day 6, the highest corrosion rate was observed with a value of 38.7 mm/y. This was a significant increase in corrosion rate compared to the low corrosion rate of 0.40 mm/y observed in the system without bacteria. This supported the SEM images in Figure 5d, where a combination of intergranular and uniform corrosion was seen over the entire surface. Alloy A smooth finished steel had shown to perform better than the rough finished surfaces.

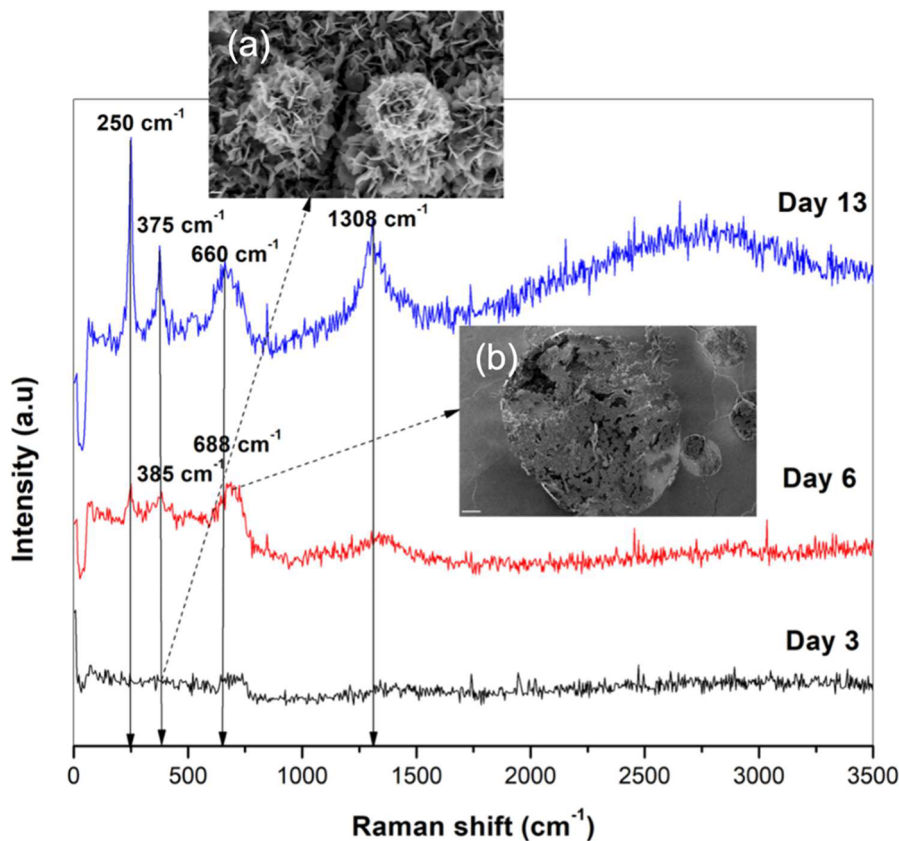
Corrosion products analysis

The evaluation of corrosion products on a carbon steel surface, gives insight on how bacterial attachment and excretion of organic acids play an important role in the corrosion process. Table 6 and Figure 7 present the Raman spectroscopy results of the alloy surface, which indicates three corrosion products including possible corrosion product mackinawite with the respective spectral peaks. The three corrosion products observed by the Raman spectra were lepidocrocite, goethite and magnetite. A phase transformation of lepidocrocite to goethite was observed in this study from day 3 at 250 cm⁻¹. This phase transformation on carbon steel was observed in a study by Balamurugan et al. [28]. Lepidocrocite was not easily evident on day 3 from the Raman spectra and rather from Figure 7 insert (a).

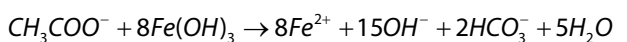
Figure 7 insert (a) revealed lepidocrocite on the surface on day 3, which was characterised as sharp flower-like structures protruding from the surface, and a similar observation was reported by Thalib et al. [36]. On day 13 lepidocrocite could be seen at intense peaks of 375 and 1308 cm⁻¹, and was also observed on day 6 at 385 cm⁻¹; however, peaks were not intense. It can be deduced that there is a mixture of lepidocrocite and goethite on day 13 possibly due to the phase transformation. Magnetite was seen more intensely on day 13 from Figure 7 insert (b) taking on the shape of dark, flat discs; this was observed by the Raman shift of 660 cm⁻¹. Magnetite peaks only started to form from day 6 and was observed as intense peaks on day 13. This was particularly observed from the SEM images (Figure 5e), where intergranular attack was alleviated on the smooth surface (day 13) and some grain boundaries were still visible. This means that the magnetite layer protected the steel surface from further corrosion. There were no magnetite peaks observed on day 3, which further infers that higher corrosion rates could be expected from day 3 and 6 (Table 5).

Table 6. Corrosion products formation of alloy a after bacterial exposure.

Corrosion product	Exposure time in days	Wavenumber (cm ⁻¹) observed in this study	Values close to reference below	Notes
Lepidocrocite (γ -FeOOH)	Day 3 (no Raman peak, deduced from SEM (Figure 5), and day 6, day 13 (most intense bands)	375 cm ⁻¹ , 1308 cm ⁻¹	Antunes et al. [31]	Kartsonakis and Charitidis [32], reported values of 393 cm ⁻¹ .
Goethite (α -FeOOH) Mackinawite	Day 13 (Sharp intense peak) and day 6 (not intense).	250 cm ⁻¹	Genchev and Erbe [33] and Leban and Kosec [34]	Kartsonakis and Charitidis [32], reported a value of 273 cm ⁻¹ for goethite. Genchev and Erbe [33], reported 253 cm ⁻¹ for mackinawite.
Magnetite (Fe ₃ O ₄)	Day 6 and day 13 (very broad)	688 cm ⁻¹ , 660 cm ⁻¹	Colomban et al. [35], Antunes et al. [31], Genchev and Erbe [33]	Kartsonakis and Charitidis [32], reported a value of 683 cm ⁻¹ .

**Figure 7.** Raman spectra of smooth alloy A after exposure on day 3, 6 and 13, with inserts indicating lepidocrocite (a) and magnetite (b).

Iron-reduction by *Clostridium* sp. and *Pseudomonas* sp. were probably involved in the formation of Fe₃O₄ (Magnetite). Organic acids played an important role, as described by Equation 2 [37]. The presence of the acid can be confirmed by the Fourier transform infrared spectroscopy results and, will be presented in the next section.



(2)

Key functional groups

FTIR has been used to study films on alloy surfaces by the absorption and transmission of infrared radiation; molecular fingerprints can be obtained. In this study, the transmission mode was used to obtain the spectra. The higher energy region (higher than 1500 cm⁻¹), can be used to determine the presence of functional groups in a molecule. The results in Figure 8 and Table 7 indicated that there were only slight differences in peak intensity over day 3, 6 and 13, where day 13

showed more intense peaks of carbonyls. There was an intense peak of acetylenic compounds observed on day 3.

It was observed that acetylenic compounds in the form of acetic acid were detected most intensely on the surface of the alloy from early stages of exposure (day 3 and day 6), in the region of $2500\text{--}2000\text{cm}^{-1}$. Corrosion results (Table 5) indicated high corrosion rates on day 6. A decrease in corrosion rate was observed on day 13. This was supported by the less intensified acetylenic peak on day 13 (Figure 8). The carbonyl peak was seen to have formed from day 3 and intensified on day 6 only. The intensified metal carbonyl peak on day 6 gives indication of C-Fe bonds. This shows further evidence that the carbon-metal bonding is a possible phenomenon. The bacteria had produced acetic acid which is a mechanism of corrosion.

Discussion

From this study it was observed that a significant proportion of the microbial diversity in the petrochemical industry has not been identified. This was evidenced during middle colonisation where an abundance of 47% (Table 1) of unknown bacteria was present on the

smooth surface of the alloy. The Vaal River supplied water to a Vaal reservoir by the use of a pumping abstraction system, which pumped water to a main reservoir. Water was then diverted to a third reservoir which supplied the petrochemical cooling towers. The change in physical environment, storage capacity and hydraulic conditions, has been reported to affect the microbial communities and microbial growth in water distribution systems [39,40]. At the current pace of discovery and characterisation, it would take some years to describe the remaining unknown species [41]. *Comamonas* sp. were seen in the gas and pipelines industry, observed with other microbial communities and were not reported to be associated with corrosion [10]. *Comamonas* sp. was observed during the late stages of attachment on the rough surface, indicating cell attachment to the already present bacteria and biofilm.

As the biofilm develops, the diverse organisms living in the EPS matrix interact according to the organisations of the biofilms. This enables the exchange of metabolites, signalling molecules, genetic material and defence compounds, organising interactions among organisms. There is competition among cells in biofilms which involves killing mechanisms or strategies that compromise growth, such as nutrient depletion or

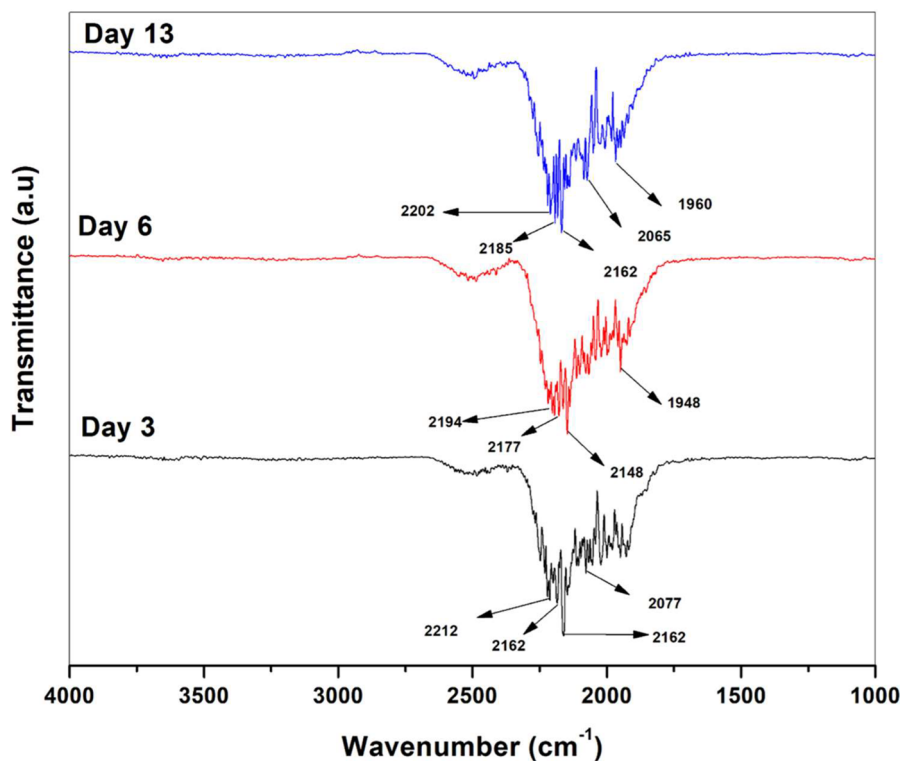


Figure 8. FTIR spectra of alloy A day 3 showing acetylenic compounds stretching at 2162cm^{-1} . Day 6 showing the acetylenic compound peak was less intensified (2148cm^{-1}), and the carbonyl peak was still present at 1948cm^{-1} . Day 13 showing acetylenic compounds at a stretch of 2162cm^{-1} , indicating decreased amounts of acetic acid produced by the bacteria.

Table 7. Functional groups.

Origin	Group frequency wavenumber cm^{-1}	Group frequency wavenumber cm^{-1} from literature	Assignment	References
C≡C	2212, 2162, 2183, 2194, 2177, 2148, 2202, 2185, 2162	2260–2100	Acetylenic compounds	Coates [38]
Transition metal carbonyls	2077, 1948, 2085, 1960	2100–1800	Transitional metal carbonyls	Coates [38]

communication mechanisms influencing biofilm composition. The autoinducer molecules of the bacterial cells are used as a communication mechanism called quorum sensing, which contribute to the adaptation *via* the EPS [42]. Moreover, incubation time has shown to influence the biofilm composition as seen in Table 1, similar to the findings observed in the study by Park et al. [17].

The presence of the bacterial species *Desulfotomaculum aeronauticum* and *Delftia* at the later growth stages has also been previously observed in industrial systems and associated with corrosion [43]. *Streptococcus* representatives observed on day 3 here, have been commonly reported to influence dental surfaces [44]. There are limited reports on the corrosive effects of the *Streptococcus* genus on industrial grade steels. *Streptococcus* sp. was reported to produce thin biofilms of about 11 μm on surfaces during early attachment stages [45]. Our findings (Table 1) are in agreement with the study conducted by [45].

The RMS roughness of the smooth finished surface increased from $8.68 \pm 1.24 \text{ nm}$ (before bacterial exposure), to $114.67 \pm 10.69 \text{ nm}$ (after bacterial exposure). The increase of the RMS roughness value may be attributed to the initial bacterial attachment and biofilm development. However, bacterial attachment may be higher on the rougher surface, inferring that the biofilm developed at an accelerated rate, most likely due to friction at the surface and larger surface area [13]. This resulted in a smooth textured biofilm layer developing initially, accompanied by an RMS roughness value of $70.70 \pm 2.1 \text{ nm}$ observed on day 3.

It was observed that *Clostridium* sp. may be the reason for the intergranular corrosion attack owing to the fact that this species was seen to dominate the smooth surface finish (Table 1). Preferential attachment and synergistic behaviour of both *Clostridium* sp. and *Pseudomonas* sp. facilitated a more severe combination of intergranular and uniform corrosion attack on visual observation. This is supported by the relative

abundance of this species on the rough surface during the initial attachment stages (Table 1).

From the corrosion rate evaluation, it was determined that A106GB smooth finished steel was identified as the best candidate steel in this bacterial system. It is to be noted that this specific material is susceptible to pitting corrosion when exposed to bacteria using rough industry standard surface finishes, as reported in a study using accelerated corrosion methods [9]. Pitting corrosion was not observed after cleaning the surfaces (Figure 5), as this is visually indicated by rounded bright cavities or holes which are produced on the steel surface. This may be due to the type of bacteria which attached to the surface. Instances of high corrosion rates and mass increase on day 3 and day 6 on the rough surfaces specifically, may be due to the synergistic behaviour of *Pseudomonas* sp. and *Clostridium* sp. [46]. which attached to the rough surface on day 3 and 6 (Table 1). The results presented in Table 1 above are in agreement with the findings from Xi et al. [1]. In the current study, *Pseudomonas* sp. was shown to grow rapidly from day 3 and representatives of this genus are capable of producing organic acids from as early as day 1 of growth [1]. The decrease in corrosion rates observed after long-term exposure (day 13) are likely due to the formation of a biofilm layer by *Pseudomonas* sp. that alleviated the corrosion rate Xi et al. [1]. However, *Clostridium* sp. and *Pseudomonas* sp. together play an important role in the protection of steel during long-term exposure by formation of a magnetite layer and similar findings were previously reported in the study by Balamurugan et al. [28]. Corrosion products such as lepidocrocite, goethite and magnetite on carbon steel were reported in another study by Refait et al. [47].

The FeS peaks (sharp and intense) observed by Raman spectroscopy were reported between 200 and 375 cm^{-1} . In this study, peaks were observed from day 6 to day 13 at 250 cm^{-1} and 375 cm^{-1} . On day 6, blackening of the batch reactor media (inoculated with bacteria) was observed. It was reported that *Clostridium* sp. are capable of producing sulphide during growth, thereby increasing iron reduction [21,48]. This was further supported by the Raman spectra, where mackinawite was observed at 250 cm^{-1} . Elemental mapping results showed a rapid decrease in iron content on the surface to 46.91% (Table 4) with indication of the presence of sulphur (Table 3). Moreover, it was seen that the abiotic media without bacteria showed blackening only on day 13 this could be due to lactate being an electron donor. When sulphide reacts with iron, black ferrous sulphide is produced. It is known that the

electron donor was from both lactate (lactic acid $C_3H_6O_3$) and metal [49].

Attachment of the abundant bacteria *Clostridium* sp. and *Pseudomonas* sp., along with their metabolites, played an important role in the corrosion kinetics of steel. Functional groups further suggested that acetylenic compounds as a metabolite were probably responsible for the accelerated corrosion rates seen on day 3 and day 6 [1].

Limitations

Characterisation of the unknown bacterial species from this petrochemical cooling water system was limited in this work. More understanding into the bacterial spatial distribution and multispecies biofilm development on surface finishes, and its impact on the corrosion rate was limited in this study. Surface energy in relation to surface hydrophobicity and surface chemistry (functional groups, electrostatic charge, and coatings) was limited in this work. The pGEM-T plasmid that was used to quantify bacterial levels only confirmed that in a multispecies system, there are no significant time-related differences in colonisation of the surfaces. However, as the results of this study suggests, more focus should be given towards quantifying the early bacterial colonisers.

Future work

Future work can be done in identifying the unknown species to understand their ecology and impacts in the petrochemical industry. Further research on carbon-metal bonding on these alloys will be worthwhile. In this study, it was impractical to conduct in-situ studies. Implementation of a modified coupon rack may be designed to hold multiple coupons for analysis on different days. Early and middle colonisation should be taken into account. This includes implementation of sterile conditions for assessment of coupons. Bacterial growth and attachment should be evaluated in conditions where the medium contains hydrocarbons. Additional qPCR work can be done by manufacturing a specialised plasmid to quantify the abundant *Clostridium* sp. on the different surfaces on day 3 early colonisation [17]. As it was observed in this study, the absolute bacterial levels using the pGEM-T plasmid showed no significant time-related differences ($p > 0.05$). This information can be used in the industry to control biofilm formation on steel through dosing strategies, especially during new installations with focus on targeting attachment of the abundant

bacteria. It may be impractical to implement smooth surfaces on all heat exchangers tubes; however, the smooth surfaces can be employed in areas of the heat exchangers where cooling water (flowing on the shell side) is stagnant such as behind the baffle plates.

Conclusions

This study focused on the petrochemical industry and focused on multispecies bacterial interactions on industry standard steel surfaces. In this study, there were no significant time-related differences on the species abundance and bacterial levels on surfaces. However, on day 3 the abundant *Clostridium* sp. was more prevalent on the rough finished surface. Time-related differences were observed on the RMS roughness values with no significant differences on the microbial corrosion rates on rough and smooth groups. Visually, the abundant strains facilitated a more severe combination of corrosion attack. Presence of acetylenic compounds and sulphur, induced high corrosion rates. Long-term exposure of the steel to bacteria showed reduced corrosion rates by formation of a magnetite film, which involved the bacterial metabolism.

Furthermore, *Pseudomonas* sp. were seen to preferentially attach to the rough surfaces, indicating higher corrosion rates than the smooth surface. The methods employed in the study highlighted the importance of conducting third generation sequencing in determining the key role players responsible for corrosion. Smooth steel A 106GB proved to perform best in this bacterial system and should be considered by the petrochemical industry during future installations.

Acknowledgements

The authors would like to extend our gratitude to the Microscopy Unit at the University of Pretoria for performing the advanced microscopy and image analysis.

Author contributions

Conceptualization, A.P.; methodology, A.P.; software, E.C.; formal analysis, A.P.; investigation, A.P.; resources, S.T, E.C. and J.N; writing—original draft preparation, A.P.; writing—review and editing, E.C, S.T. and J.N; supervision, E.C and S.T.; project administration, E.C and S.T.; funding acquisition, E.C and S.T. All authors have read and agreed to the published version of the manuscript.

Disclosure statement

No potential conflict of interest was reported by the author(s).

Funding

The authors would like to thank the National Research Fund (NRF) of South Africa for funding the project through the Grant No's SRUG2204072544 and EQP180503325881. Authors thank the NRF for additional funding provided via the Thuthuka Grant No. TTK18024324064.

Data availability statement

Data will be made available upon request through the corresponding author and/or the director of the project, Prof. Evans Chirwa (Email: evans.chirwa@up.ac.za).

References

- [1] Xi G, Zhao X, Wang S, et al. Synergistic effect between sulfate-reducing bacteria and *Pseudomonas aeruginosa* on corrosion behavior of Q235 steel. *Int J Electrochem Sci.* 2020;15(1):1–18. doi: [10.20964/2020.01.38](https://doi.org/10.20964/2020.01.38).
- [2] Achinas S, Charalampogiannis N, Euverink GJW. A brief recap of microbial adhesion and biofilms. *Appl Sci.* 2019;9(14):2801. doi: [10.3390/app9142801](https://doi.org/10.3390/app9142801).
- [3] Tuck B, Watkin E, Forsyth M, et al. Evaluation of a novel, multi-functional inhibitor compound for prevention of biofilm formation on carbon steel in marine environments. *Sci Rep.* 2021;11(1):15697. doi: [10.1038/s41598-021-94827-9](https://doi.org/10.1038/s41598-021-94827-9).
- [4] Graham MV, Cady NC. Nano and microscale topographies for the prevention of bacterial surface fouling. *Coatings.* 2014;4(1):37–59. doi: [10.3390/coatings4010037](https://doi.org/10.3390/coatings4010037).
- [5] Leonard H, Jiang X, Arshavsky-Graham S, et al. Shining light in blind alleys: deciphering bacterial attachment in silicon microstructures. *Nanoscale Horiz.* 2022;7(7):729–742. doi: [10.1039/d2nh00130f](https://doi.org/10.1039/d2nh00130f).
- [6] Santos ALS, Galdino ACM, Mello TPD, et al. What are the advantages of living in a community? A microbial biofilm perspective! *Mem Inst Oswaldo Cruz.* 2018;113(9):1–7. doi: [10.1590/0074-02760180212](https://doi.org/10.1590/0074-02760180212).
- [7] Queiroz GAD, Andrade JS, Malta TBS, et al. Biofilm formation and corrosion on carbon steel API 5LX60 in clayey soil. *Mater Res.* 2018;21(3):e20170338.
- [8] Tang M, Chen C, Zhu J, et al. Inhibition of bacterial adhesion and biofilm formation by a textured fluorinated alkoxyphosphazene surface. *Bioact Mater.* 2021;6(2):447–459.
- [9] Prithiraj A, Otunniyi IO, Osifo P, et al. Corrosion behaviour of stainless and carbon steels exposed to sulphate-reducing bacteria from industrial heat exchangers. *Eng Fail Anal.* 2019;104:977–986. doi: [10.1016/j.engfailanal.2019.06.042](https://doi.org/10.1016/j.engfailanal.2019.06.042).
- [10] Zhu XY, Lubeck J, Kilbane JJ. Characterization of microbial communities in gas industry pipelines. *Appl Environ Microbiol.* 2003;69(9):5354–5363. doi: [10.1128/AEM.69.9.5354-5363.2003](https://doi.org/10.1128/AEM.69.9.5354-5363.2003).
- [11] Procópio L. The oil spill and the use of chemical surfactant reduce microbial corrosion on API 5L steel buried in saline soil. *Environ Sci Pollut Res.* 2021;28(21):26975–26989. doi: [10.1007/s11356-021-12544-2](https://doi.org/10.1007/s11356-021-12544-2).
- [12] Bohinc K, Dražič G, Oder M, et al. Available surface dictates microbial adhesion capacity. *Int J Adhes Adhes.* 2014;50:265–272. doi: [10.1016/j.ijadhadh.2014.01.027](https://doi.org/10.1016/j.ijadhadh.2014.01.027).
- [13] Nouri A, Shirvan AR, Li Y, et al. Surface modification of additively manufactured metallic biomaterials with active antipathogenic properties. *Smart Mater Manuf.* 2023;1:100001. doi: [10.1016/j.smmf.2022.100001](https://doi.org/10.1016/j.smmf.2022.100001).
- [14] Bauer S, Arpa-Sancet MP, Finlay JA, et al. Adhesion of marine fouling organisms on hydrophilic and amphiphilic polysaccharides. *Langmuir.* 2013;29(12):4039–4047. doi: [10.1021/la3038022](https://doi.org/10.1021/la3038022).
- [15] Yoda I, Koseki H, Tomita M, et al. Effect of surface roughness of biomaterials on *Staphylococcus epidermidis* adhesion. *BMC Microbiol.* 2014;14(1):234. doi: [10.1186/s12866-014-0234-2](https://doi.org/10.1186/s12866-014-0234-2).
- [16] Dezelic T, Schmidlin PR. Multi-species biofilm formation on dental materials and an adhesive patch. *Oral Health Prev Dent.* 2009;7(1):47–53.
- [17] Park JW, An JS, Lim WH, et al. Microbial changes in biofilms on composite resins with different surface roughness: an in vitro study with a multispecies biofilm model. *J Prosthet Dent.* 2019;122(5):493–4e1.
- [18] Yuan L, Hansen MF, Røder HL, et al. Mixed-Species biofilms in the food industry: current knowledge and novel control strategies. *Crit Rev Food Sci Nutr.* 2020;60(13):2277–2293. doi: [10.1080/10408398.2019.1632790](https://doi.org/10.1080/10408398.2019.1632790).
- [19] Kuwada N, Fujii Y, Nakatani T, et al. Diamond-like carbon coating to inner surface of polyurethane tube reduces *Staphylococcus aureus* bacterial adhesion and biofilm formation. *J Artif Organs.* 2023;1–9. PMID: 37227545. doi: [10.1007/s10047-023-01403-1](https://doi.org/10.1007/s10047-023-01403-1).
- [20] Prithiraj A, Tichapondwa S, Chirwa EM. Kinetic growth model and metabolic effect of a bacterial consortia from a petrochemical processing plant. *Can J Chem Eng.* 2023;1–11. doi: [10.1002/cjce.25154](https://doi.org/10.1002/cjce.25154).
- [21] Dwivedi D, Lepková K, Becker T. Carbon steel corrosion: a review of key surface properties and characterization methods. *RSC Adv.* 2017;7(8):4580–4610. doi: [10.1039/C6RA25094G](https://doi.org/10.1039/C6RA25094G).
- [22] Zhao M, Tyson C, Chen HC, et al. *Pseudomonas allivivorans* sp. nov., a plant-pathogenic bacterium isolated from onion foliage in Georgia, USA. *Syst Appl Microbiol.* 2022;45(1):126278. doi: [10.1016/j.syapm.2021.126278](https://doi.org/10.1016/j.syapm.2021.126278).
- [23] Makuwa S, Green E, Fosso-Kankeu E, et al. A snapshot of the influent and effluent bacterial populations in a wastewater treatment plant in the North-West province, South Africa. *Appl Microbiol.* 2023;3(3):764–773. doi: [10.3390/applmicrobiol3030053](https://doi.org/10.3390/applmicrobiol3030053).
- [24] Kadaifciler DG, Unsal T, Ilhan-Sungur E. Long-term evaluation of culturable fungi in a natural aging biofilm on galvanized steel surface. *Johnson Matthey Technol Rev.* 2024;6:1–27.
- [25] Kumar H, Sharma S, Kumari R. Corrosion inhibition and adsorption mechanism of morus nigra on mild steel in acidic medium: a sustainable and green approach. *Vietnam J Chem.* 2022;60(4):417–434.
- [26] Jeong G, Kim HJ, Kim KE, et al. Selective attachment of prokaryotes and emergence of potentially pathogenic prokaryotes on four plastic surfaces: adhesion study in a natural marine environment. *Mar Pollut Bull.* 2023;193:115149. doi: [10.1016/j.marpolbul.2023.115149](https://doi.org/10.1016/j.marpolbul.2023.115149).
- [27] Wang J, Yin Y. Clostridium species for fermentative hydrogen production: an overview. *Int J Hydrogen Energy.* 2021;46(70):34599–34625. doi: [10.1016/j.ijhydene.2021.08.052](https://doi.org/10.1016/j.ijhydene.2021.08.052).

- [28] Balamurugan P, Chandramohan P, Rao TS. Corrosion management of carbon steel material: operational modes influence corrosion rate—an in vitro study. *RSC Adv.* 2016;6(47):41122–41129. doi: [10.1039/C6RA01070A](https://doi.org/10.1039/C6RA01070A).
- [29] Kim SK, Park IJ, Lee DY, et al. Influence of surface roughness on the electrochemical behavior of carbon steel. *J Appl Electrochem.* 2013;43(5):507–514. doi: [10.1007/s10800-013-0534-5](https://doi.org/10.1007/s10800-013-0534-5).
- [30] Martin WF. Carbon–metal bonds: rare and primordial in metabolism. *Trends Biochem Sci.* 2019;44(9):807–818. doi: [10.1016/j.tibs.2019.04.010](https://doi.org/10.1016/j.tibs.2019.04.010).
- [31] Antunes RA, Ichikawa RU, Martinez LG, et al. Characterization of corrosion products on carbon steel exposed to natural weathering and to accelerated corrosion tests. *Int J Corros.* 2014;2014:1–9. doi: [10.1155/2014/419570](https://doi.org/10.1155/2014/419570).
- [32] Kartsonakis IA, Charitidis CA. Corrosion protection evaluation of mild steel: the role of hybrid materials loaded with inhibitors. *Appl Sci.* 2020;10(18):6594. doi: [10.3390/app10186594](https://doi.org/10.3390/app10186594).
- [33] Genchev G, Erbe A. Raman spectroscopy of mackinawite FeS in anodic iron sulfide corrosion products. *J Electrochem Soc.* 2016;163(6):C333–C338. doi: [10.1149/2.1151606jes](https://doi.org/10.1149/2.1151606jes).
- [34] Leban MB, Kosec T. Characterization of corrosion products formed on mild steel in deoxygenated water by raman spectroscopy and energy dispersive X-ray spectrometry. *Eng Fail Anal.* 2017;79:940–950. doi: [10.1016/j.engfailanal.2017.03.022](https://doi.org/10.1016/j.engfailanal.2017.03.022).
- [35] Colomban P, Cherifi S, Despert G. Raman identification of corrosion products on automotive galvanized steel sheets. *J Raman Spectroscopy.* 2008;39(7):881–886. doi: [10.1002/jrs.1927](https://doi.org/10.1002/jrs.1927).
- [36] Thalib S, Ikhsan M, Fonna S, et al. Identification of corrosion product on medium carbon steel under the exposure of banda aceh's atmosphere. *IOP Conf Ser: Mater Sci Eng.* 2018;352(1):012004. doi: [10.1088/1757-899X/352/1/012004](https://doi.org/10.1088/1757-899X/352/1/012004).
- [37] Sun H, Shi B, Lytle DA, et al. Formation and release behavior of iron corrosion products under the influence of bacterial communities in a simulated water distribution system. *Environ Sci Process Impacts.* 2014;16(3):576–585. doi: [10.1039/c3em00544e](https://doi.org/10.1039/c3em00544e).
- [38] Coates J. Interpretation of infrared spectra, a practical approach. Chichester: Wiley; 2000. p. 10815–10837.
- [39] Cheng B, Xia R, Zhang Y, et al. Characterization and causes analysis for algae blooms in large river system. *Sustainable Cities Soc.* 2019;51:101707. doi: [10.1016/j.scs.2019.101707](https://doi.org/10.1016/j.scs.2019.101707).
- [40] Guo J, Zheng Y, Teng J, et al. Characteristics of spatial distribution for microbial ecology inside and outside source water reservoir. *J Clean Prod.* 2021;311:127697. doi: [10.1016/j.jclepro.2021.127697](https://doi.org/10.1016/j.jclepro.2021.127697).
- [41] Bouchet P, Decock W, Lonnaville B, et al. Marine biodiversity discovery: the metrics of new species descriptions. *Front Mar Sci.* 2023;10:929989. doi: [10.3389/fmars.2023.929989](https://doi.org/10.3389/fmars.2023.929989).
- [42] Smith WP, Wucher BR, Nadell CD, et al. Bacterial defences: mechanisms, evolution and antimicrobial resistance. *Nat Rev Microbiol.* 2023;21(8):519–534. doi: [10.1038/s41579-023-00877-3](https://doi.org/10.1038/s41579-023-00877-3).
- [43] Critchley M, Javaherdashti R. 2004. Metals, microbes and MIC—a review of microbiologically influenced corrosion. In: *Proceedings of Corrosion and Prevention*, Perth, Australia. p. 1–8. CAP04.
- [44] Bender O, Houry J, Hirsch G, et al. Immunorecognition of *Streptococcus mutans* secreted proteins protects against caries by limiting tooth adhesion. *J Dent.* 2024;141:104805. doi: [10.1016/j.jdent.2023.104805](https://doi.org/10.1016/j.jdent.2023.104805).
- [45] Rozen R, Bachrach G, Zachs B, et al. Growth rate and biofilm thickness of *Streptococcus sobrinus* and *Streptococcus mutans* on hydroxapatite. *APMIS.* 2001;109(2):155–160. doi: [10.1034/j.1600-0463.2001.d01-117.x](https://doi.org/10.1034/j.1600-0463.2001.d01-117.x).
- [46] Tiburcio SRG, Macrae A, Peixoto RS, et al. Sulphate-reducing bacterial community structure from produced water of the periquito and galo de campina onshore oilfields in Brazil. *Sci Rep.* 2021;11(1):20311. doi: [10.1038/s41598-021-99196-x](https://doi.org/10.1038/s41598-021-99196-x).
- [47] Refait P, Grolleau AM, Jeannin M, et al. Corrosion of carbon steel in marine environments: role of the corrosion product layer. *Corros Mater Degrad.* 2020;1(1):198–218. doi: [10.3390/cmd1010010](https://doi.org/10.3390/cmd1010010).
- [48] Shah M. Iron oxide reduction by *clostridial* consortium: insights from physiological and genome analysis [PhD thesis]. New Brunswick (NJ): The State University of New Jersey; 2013. p. 1–114.
- [49] Oyekola OO, van Hille RP, Harrison ST. Kinetic analysis of biological sulphate reduction using lactate as carbon source and electron donor: effect of sulphate concentration. *Chem Eng Sci.* 2010;65(16):4771–4781. doi: [10.1016/j.ces.2010.05.014](https://doi.org/10.1016/j.ces.2010.05.014).